Electronic Supplementary Information

Highly dispersed palladium nanoclusters anchored on nanostructured hafnium(IV) oxide as highly efficient catalysts for the Suzuki–Miyaura coupling reaction

Xiaoxue Wu,[a] Wenting Lin,[a] Li Wang,[a] Nan Li,[a] Gaomei Tu,[a] Yanghe Fu,[a] De-Li Chen,[a] Weidong Zhu,[a] Guihua Chen[b] and Fumin Zhang*[a]

[a]Key Laboratory of the Ministry of Education for Advanced Catalysis Materials, Institute of Physical Chemistry, Zhejiang Normal University, 321004 Jinhua, People's Republic of China

[b]School of Pharmaceutical and Material Engineering, Taizhou University, 318000 Jiaojiang People's Republic of China

[*] **Corresponding Author**: E-mail: zhangfumin@zjnu.edu.cn

1. Experimental

1.1. Chemicals

All chemicals are commercially available and used directly without any treatment: hafnium (IV) chloride (HfCl$_4$, Strem, 99.9%), zirconium (IV) tetrachloride (ZrCl$_4$, Strem, 99.9%), 2-aminoterephthalic acid (NH$_2$-BDC, TCI, >98%), palladium chloride (PdCl$_2$, TCI, 98%), hydrochloric acid (HCl, Sinopharm Chemical Reagent Co., Ltd., 37%), N, N-dimethylformamide (DMF, Sinopharm Chemical Reagent Co., Ltd., ≥99.5%), methanol (Sinopharm Chemical Reagent Co., Ltd., ≥99.5%), ethanol (Sinopharm Chemical Reagent Co., Ltd., ≥99.5%), acetic acid (Sinopharm Chemical Reagent Co., Ltd., ≥99.5%), acetonitrile (Sinopharm Chemical Reagent Co., Ltd., ≥99.5%), acetone (Sinopharm Chemical Reagent Co., Ltd., ≥99.5%), ethyl acetate (Sinopharm Chemical Reagent Co., Ltd., ≥99.5%), phenylboronic acid (C$_6$H$_7$BO$_2$, J&K, 99%), bromobenzene (C$_6$H$_5$Br, damas-beta, 98%), iodobenzene (C$_6$H$_5$I, Aldrich, 99%), chlorobenzene (C$_6$H$_5$Cl, Mreda, ≥99%), 2-bromobenzaldehyde (C$_7$H$_5$BrO, Meryer, 98%), 3-bromobenzaldehyde (C$_7$H$_5$BrO, Aldrich, 97%), 4-bromobenzaldehyde (C$_7$H$_5$BrO, Aldrich, 99%), 4-bromotoluene (C$_7$H$_7$Br, Aldrich, 99%), 2-bromotoluene (C$_7$H$_7$Br, Meryer, 99%), 4-iodotoluene (C$_7$H$_7$I, Aldrich, 99%), 4-bromoanisole (C$_7$H$_7$BrO, Aldrich, 99%), potassium carbonate (K$_2$CO$_3$, Aldrich, 99.5%), caesium carbonate (Cs$_2$CO$_3$, Meryer, 99.9%), sodium hydroxide (NaOH, Kermel, >96%), sodium carbonate (Na$_2$CO$_3$, Sinopharm Chemical Reagent Co., Ltd., ≥99.8%), natrium bicarbonate (NaHCO$_3$, Sinopharm Chemical Reagent Co., Ltd., ≥99.8%), and triethylamine (C$_6$H$_{15}$N, Aldrich, ≥99%). Deionized water with a resistance >18.2 MΩ was obtained from a Millipore

Milli-Q ultrapure water purification system. Hydrogen (H_2, Zhejiang Jinhua Wucheng Datong Gas Co., Ltd, 99.999%). Nitrogen (N_2, Zhejiang Jinhua Wucheng Datong Gas Co., Ltd, 99.999%).

1.2. Characterization

The X-ray powder diffraction (XRD) patterns were obtained on a Philips PW3040/60 diffractometer using Cu Kα radiation (λ=0.1541 nm, 40 kV, 30 mA).

N_2 adsorption isotherms were measured at -196 °C on a Micromeritics ASAP 2020 instrument. The samples were outgassed under vacuum at 200 °C for 12 h before adsorption measurement. The surface area was determined using the Brunauer-Emmett-Teller (BET) method.

The morphology of the samples were obtained by field emission SEM on a scanning electron microscope (a Hitachi S-4800 microscope) and TEM on a transmission electron microscope (JEM2100F, JEOL, Japan) working at 200 kV.

X-ray photoelectron spectroscopy (XPS) data were collected on an ESCALAB250 electron spectrometer from VG Scientific using 300 W Al-Kα radiation. The XPS data were internally calibrated, fixing the binding energy of C 1s at 284.8 eV.

The surface properties of the catalysts were measured by temperature-programmed desorption of ammonia (NH_3-TPD, a Micro-meristics AutoChem II 2920 instrument). The sample (150 mg) was purged under a flow of He of 30 mL/min at 350 °C for 2 h. After purging, the sample was cooled to 110 °C, and the feed composition was switched to a mixture containing 20% NH_3 in He (30 mL/min) for 30 min. The physisorbed ammonia was flushed out with He flow for 1 h. Afterward, the sample cell was heated at

10 °C/min under He to 900 °C. The concentration of the desorbed ammonia was monitored continuously with a TCD detector.

The amounts of the metal Pd species in the different samples were determined by an IRIS Intrepid II XSP inductively coupled plasma-atomic emission spectrometer (ICP-AES).

Electron Paramagnetic Resonance (EPR) measurement was obtained on the Bruker EPR EMXplus-9.5/12 at room temperature. The frequency and power of the microwave were set to 9.847226 GHz and 2.0000 mW, respectively. Gauss field modulation at 100 kHz and a time constant of 20 ms was used for detection.

The nuclear magnetic resonance (NMR) spectra of the products were recorded on a Bruker Avance 600 MHz spectrometer at 297 K using $CDCl_3$ (δ H=7.26, δ C=77.0) as an internal standard for ^{1}H NMR and 125 MHz for ^{13}C NMR.

1.3. Catalyst preparation

Synthesis of Pd@NH$_2$-UiO-66(Hf)

Pd@NH$_2$-UiO-66(Hf) was synthesized by a one-pot strategy according to the procedure reported in the previous papers with some slight modification.[1] Briefly, $HfCl_4$ (4.7 mmol) and NH$_2$-BDC (4.7 mmol) were dissolved in DMF (200 mL) in a round-bottom flask (500 mL in capacity) and then added acetic acid (36 mL), deionized water (5.0 mL), and $PdCl_2$ precursor (0.5 mL, 10 mg/mL) to the solution. The mixture was treated under ultrasound for 10 min to form a homogeneous solution. Afterward, the mixture was heated at 75 °C for 20 h. Subsequently, the temperature was raised to 130 °C, and the mixture was allowed to stir for another 4 h, and then cooled to room

temperature. The product was centrifugated at 9000 rpm for 4 min, washed with DMF and methanol three times, respectively, and finally dried under vacuum at 120 °C for 12 h. Other control samples, including Pd@NH$_2$-UiO-66(Zr), NH$_2$-UiO-66(Zr), and NH$_2$-UiO-66(Hf), were also synthesized by a similar method.

Synthesis of Pd/HfO$_2$@CN

The Pd/HfO$_2$@CN powders were fabricated directly via one-step pyrolysis strategy. Typically, the Pd@NH$_2$-UiO-66(Hf) precursor (0.1 g) was transferred into a tube furnace. The furnace was heated at 600 °C at a rate of 3 °C/min with nitrogen gas flow (flow rate: 100 ml/min). The furnace was held at this temperature for 3 h and then allowed to cool to room temperature. Before use, the obtained powder was further reduced in a stream of hydrogen (H$_2$)/N$_2$ (10:40 mL/min) at 250 °C for 4 h. Pd/ZrO$_2$@CN was prepared following the same procedure.
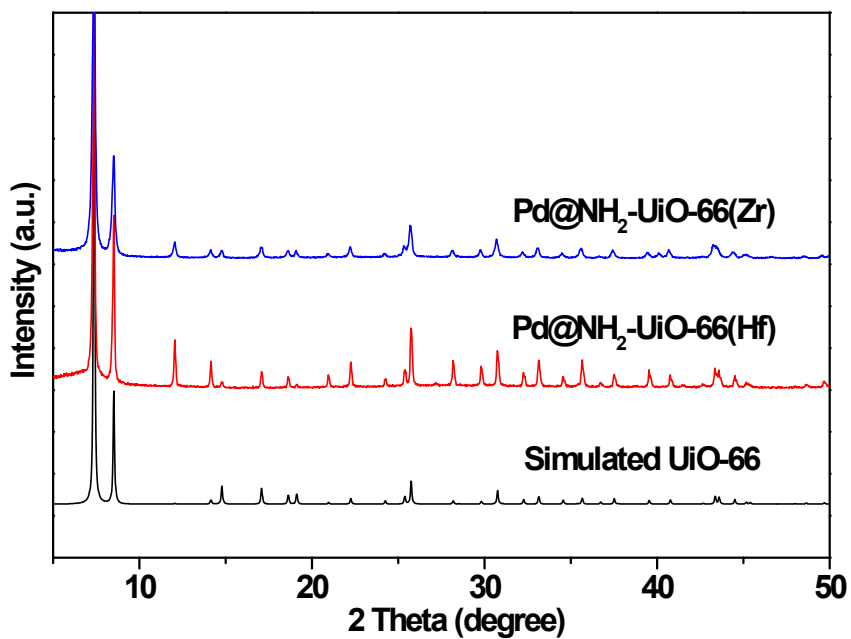
Fig. S1 XRD patterns of simulated UiO-66, the synthesized Pd@NH$_2$-UiO-66(Hf) and

Pd@NH$_2$-UiO-66(Zr).
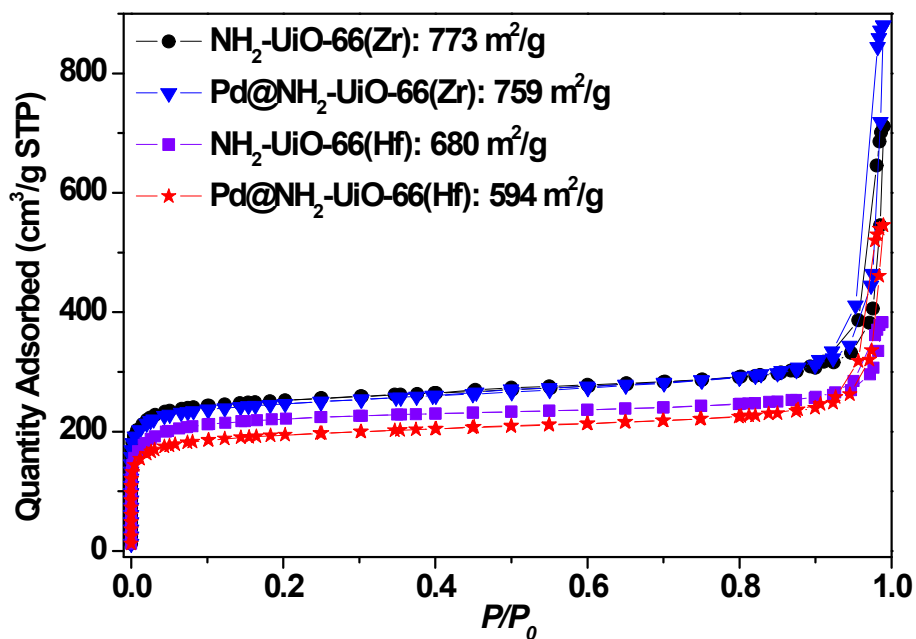
Fig. S2 N$_2$ adsorption–desorption isotherms of NH$_2$-UiO-66(Zr), Pd@NH$_2$-UiO-66(Zr), NH$_2$-

UiO-66(Hf), and Pd@NH$_2$-UiO-66(Hf).
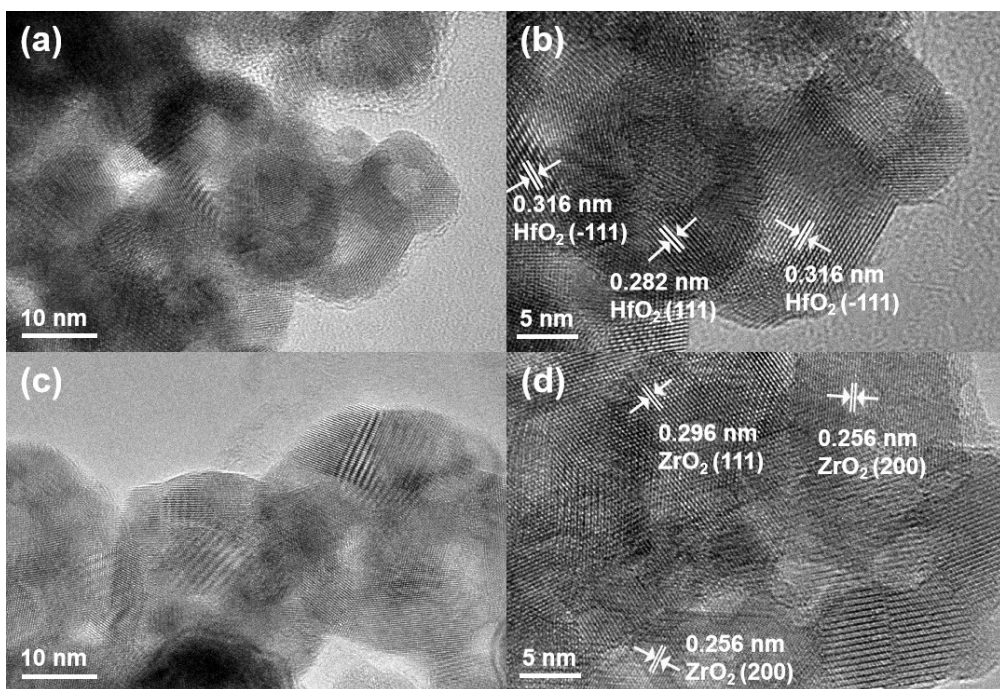
Fig. S3 TEM images of Pd@HfO$_2$ (a and b) and Pd@ZrO$_2$ (c and d).
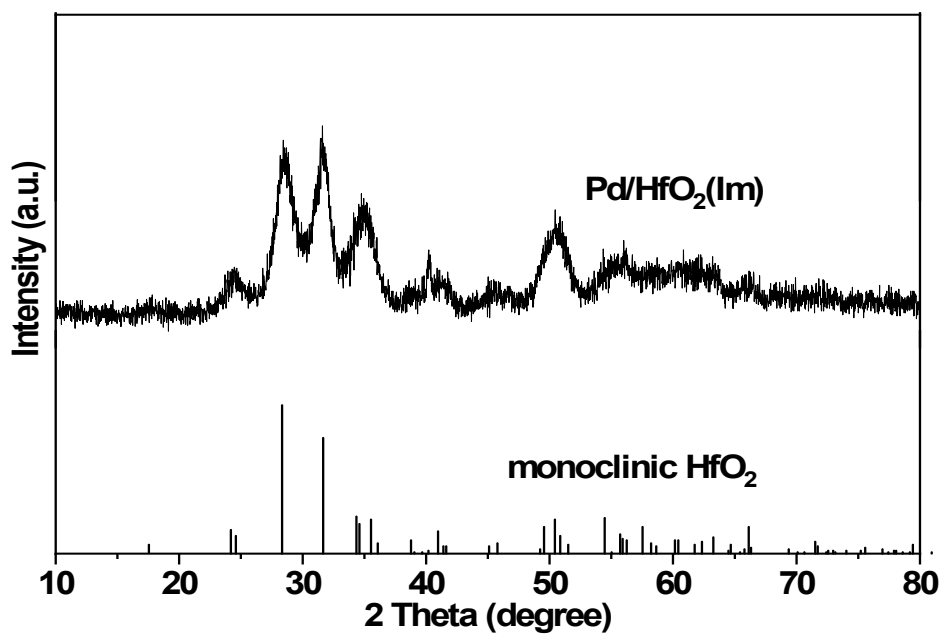
Fig. S4 XRD pattern of Pd/HfO$_2$(Im).
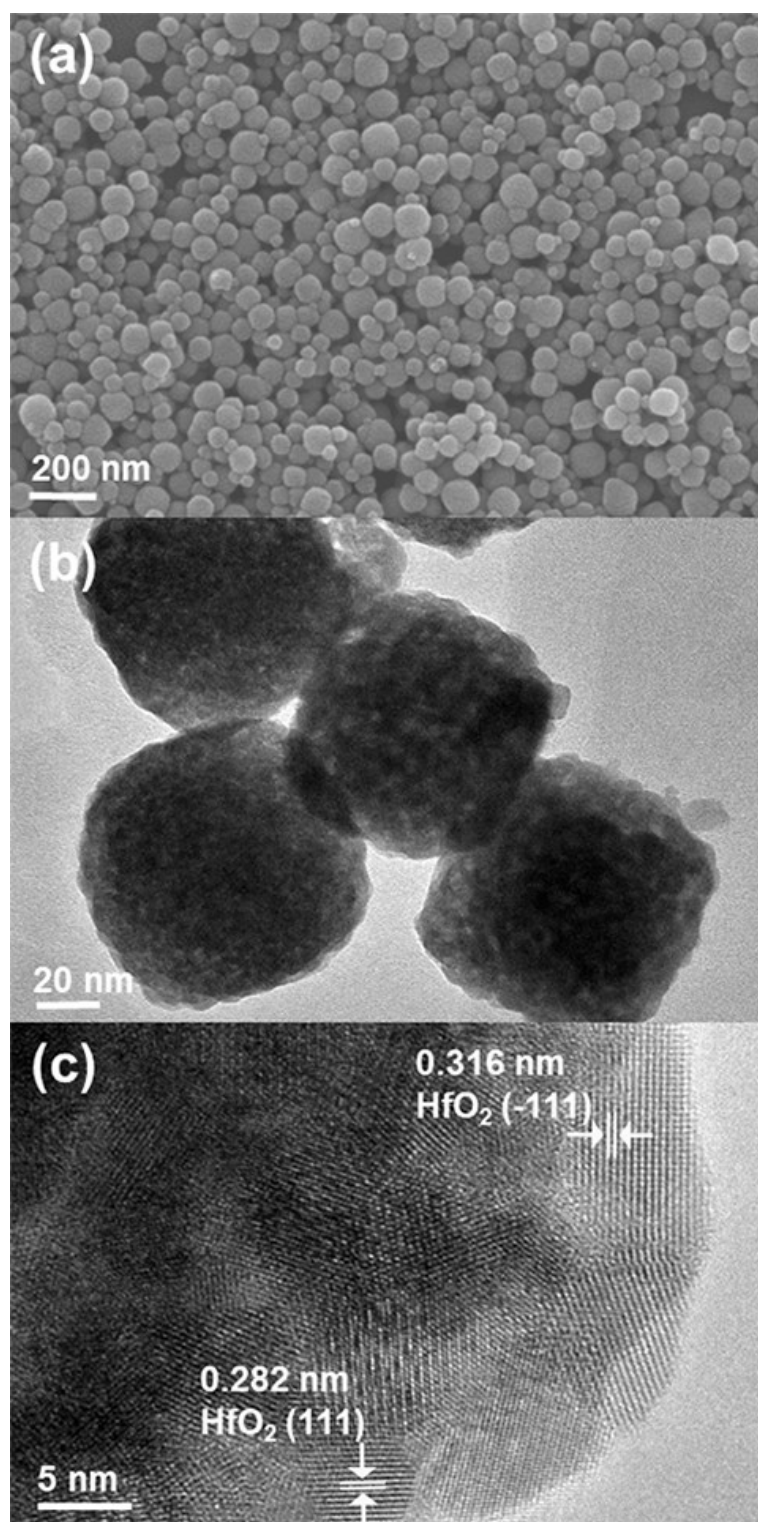
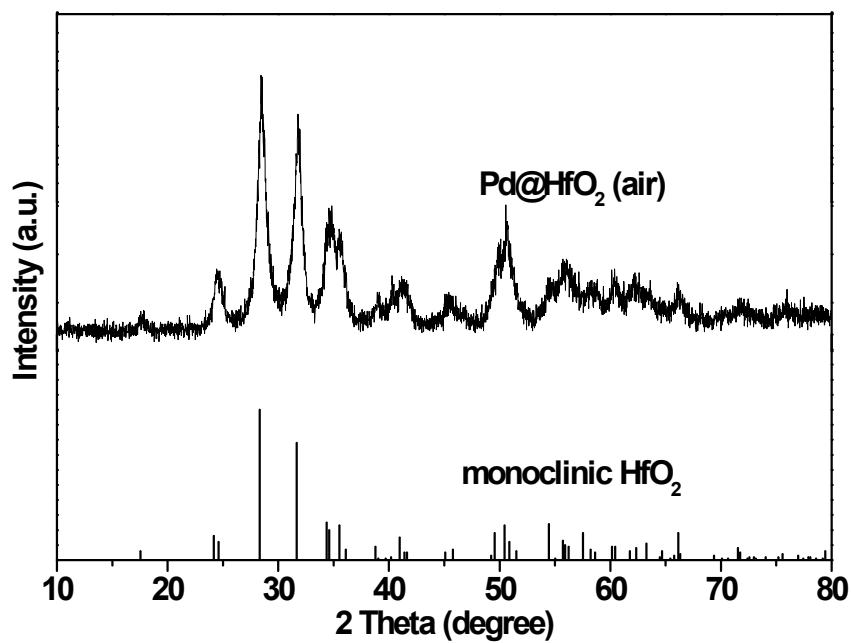**Fig. S5** SEM (a), TEM (b), and HRTEM (c) images of Pd/HfO$_2$(Im).

Fig. S6 XRD pattern of Pd@HfO$_2$(air).
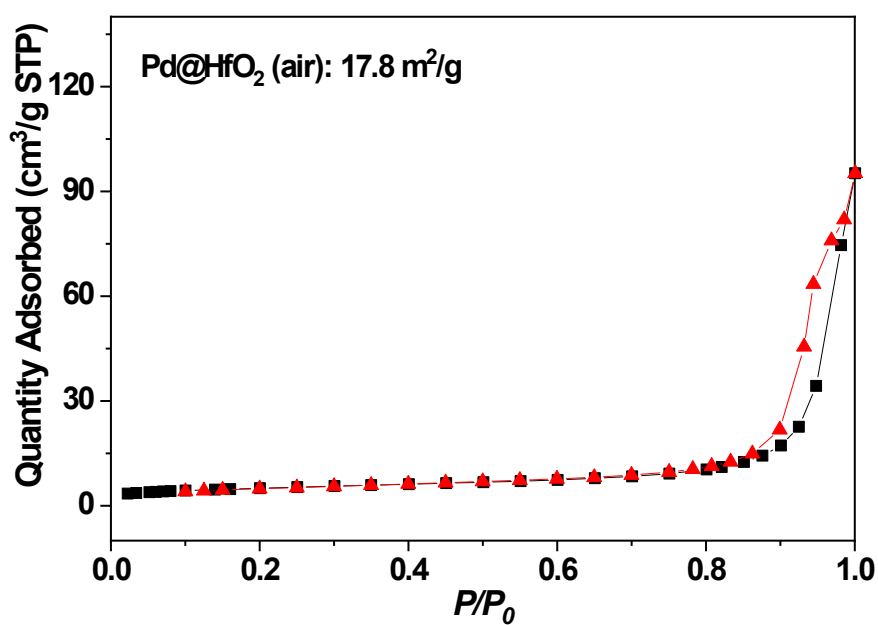
Fig. S7 N$_2$ adsorption–desorption isotherms of Pd@HfO$_2$(air).
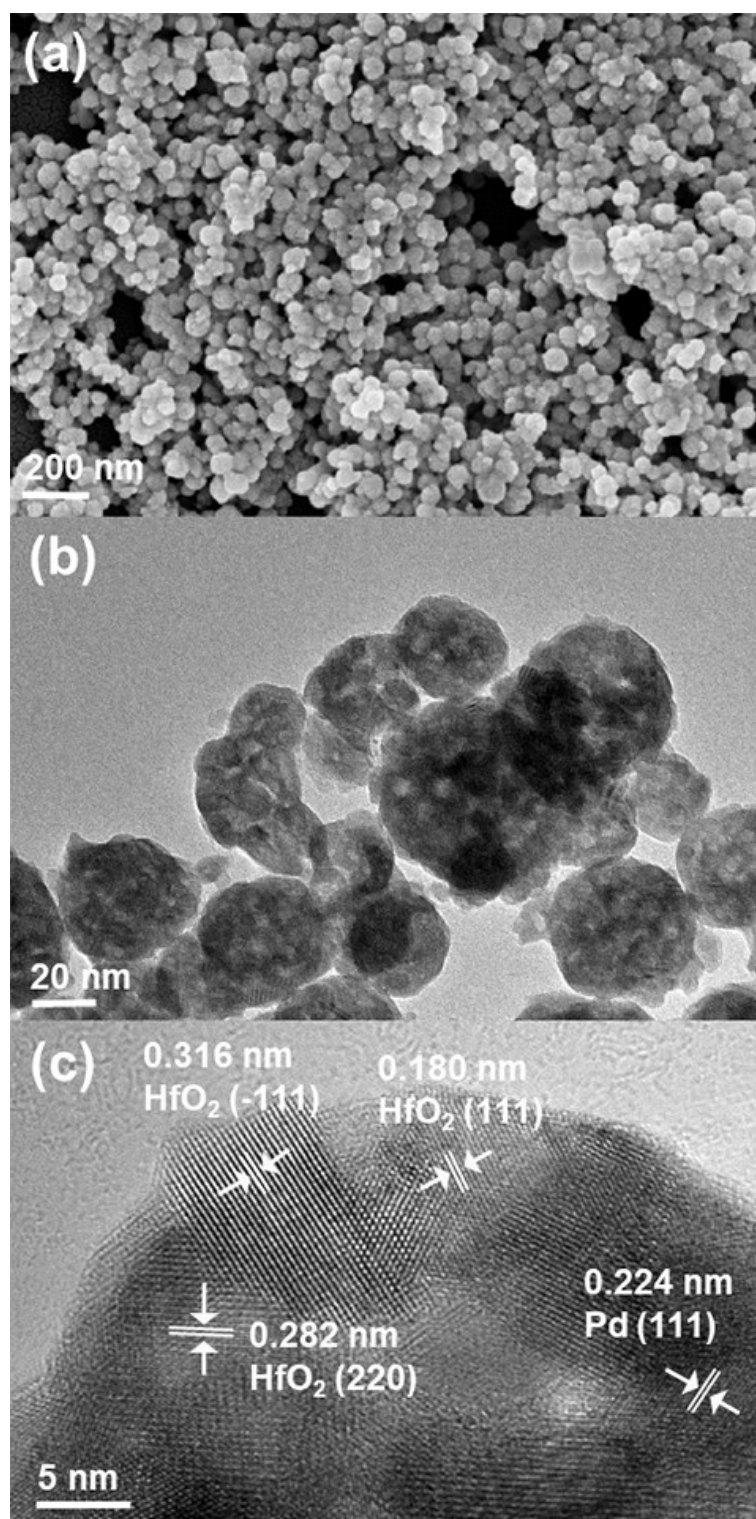
Fig. S8 SEM (a), TEM (b), and HRTEM (c) images of Pd@HfO$_2$(air).
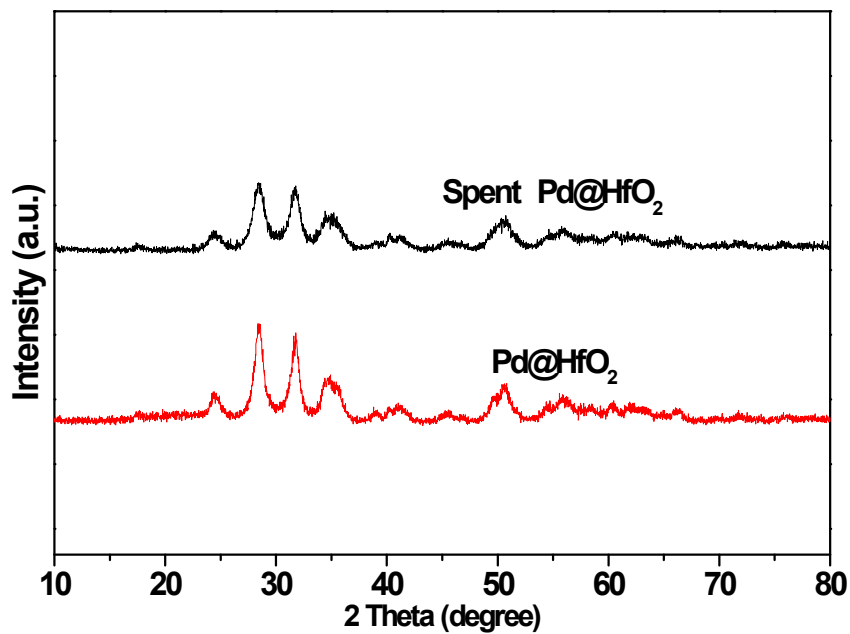
Fig. S9 XRD patterns of the fresh and used Pd@HfO$_2$ catalyst.
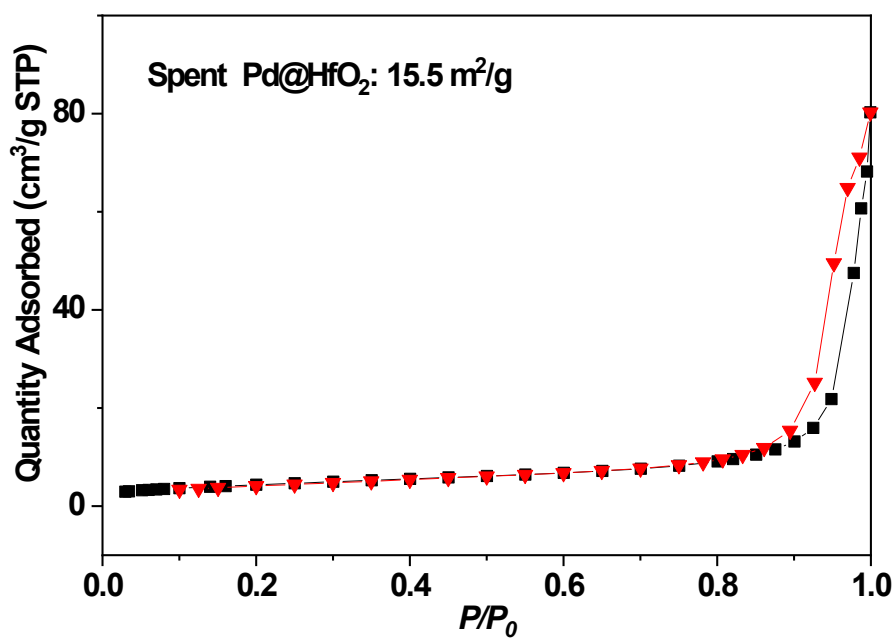
Fig. S10 N$_2$ adsorption isotherms of the spent Pd@HfO$_2$ catalyst.
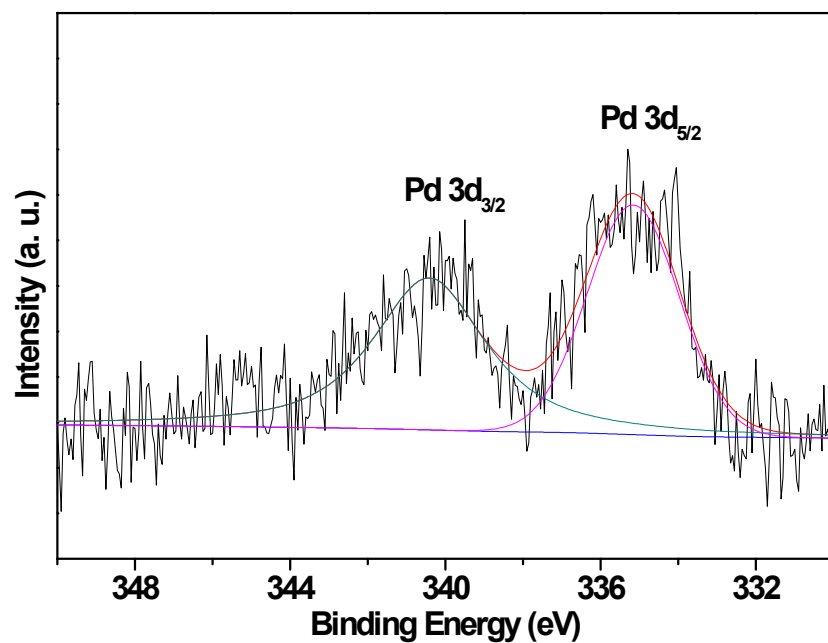
Fig. S11 High resolution XPS spectrum of Pd 3d for the spent Pd@HfO$_2$ catalyst.
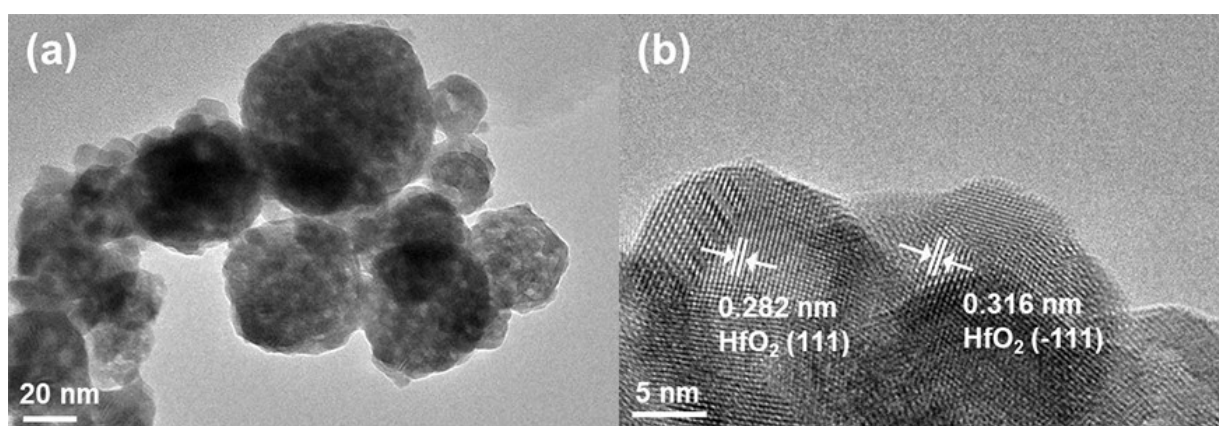
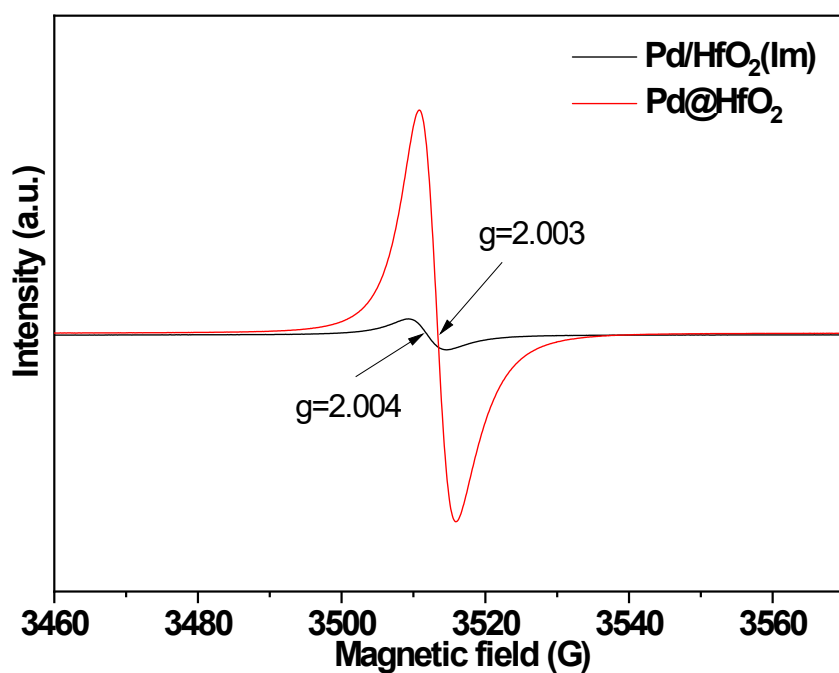**Fig. S12** TEM (a) and HRTEM (b) images of the spent Pd@HfO$_2$ catalyst.

Fig. S13 EPR spectra of Pd@HfO$_2$ and Pd/HfO$_2$(Im).

The Pd@HfO$_2$ has more oxygen vacancies in comparison with that of Pd/HfO$_2$(Im), likely owning to the strong interaction between HfO$_2$ and Pd formed during the two-step thermal treatment, which is beneficial for forming a highly stable catalyst.

Table S1 Suzuki-Miyaura cross-coupling reaction of bromobenzene and arylboronic acids using palladium catalysts

Entry	Catalyst	R	Products	T (°C)	Yield (%)
1	Pd@HfO$_2$	H		50	>99
2	Pd@NH$_2$-UiO-66(Hf)	H		50	50
3	Pd@NH$_2$-UiO-66(Zr)	H		50	41
4	Pd/HfO$_2$@CN	H		50	85
5	Pd/ZrO$_2$@CN	H		50	80
6	Pd@HfO$_2$	4-CH$_3$		80	75
7	Pd@HfO$_2$	4-OCH$_3$		80	72
8	Pd@HfO$_2$	2-CH$_3$		80	70

Reaction conditions: bromobenzene (0.32 mmol), arylboronic acid (0.38 mmol), K$_2$CO$_3$ (0.38 mmol), Ethanol/H$_2$O = 1:1 (4.0 mL), catalyst (0.1 mol%), 2 h.

Table S2 Comparison of catalytic activity for the Suzuki-Miyaura coupling reaction over different catalysts.

Entry	Catalyst	Reaction conditions Catalyst/solvent/base/temperature/time	Yield (%)	Ref.
1	Pd@HfO$_2$	0.1 mol% catalyst/EtOH: H$_2$O (1:1)/K$_2$CO$_3$ (1.2 equiv)/50 °C/2 h	>99	This work
2	Pd-Pt Nanodendrites	4 mg catalyst/EtOH: H$_2$O (1:1)/Cs$_2$CO$_3$ (1.2 equiv)/80 °C/2 h	98	2
3	Pd@porous SiO$_2$	0.003 mol% catalyst/DMF: H$_2$O (21:1)/Cs$_2$CO$_3$ (2.0 equiv)/200 °C/1 h	100	3
4	Pd/Porous-nanorods-CeO$_2$-160	0.3 mol% catalystDMF: H$_2$O (1:1)/K$_2$CO$_3$ (3.0 equiv)/90 °C/1 h	72.3	4
5	Pd@Mesopor ous Carbon	2 mol% catalyst/EtOH: H$_2$O (1:1)/Na$_2$CO$_3$ (2.0 equiv)/80 °C/1 h	98	5
6	Pd@Fluorescent Material	0.05 mol% catalyst/H$_2$O/K$_2$CO$_3$ (2.0 equiv)/80 °C/10 h	91	6
7	Pd-TiO$_2$/Carbon Nanofibers	10 mg catalyst/H$_2$O/K$_2$CO$_3$ (2.0 equiv)/50 °C/5 h	5	7
8	SiO$_2$/(Tetraethyl ene glycol)/Pd	0.75 mol% catalyst/Toluene/K$_3$PO$_4$ (2.0 equiv)/110 °C/12 h	86	8
9	Pd/SBA-15	0.2 mol% catalyst/EtOH: H$_2$O	88	9

		(1:3)/K₂CO₃ (3.0 equiv)/85°C/10 h		
10	Pd/Pr Coordination Polymers	0.4 mol% catalyst/DMF: H_2O (1:1)/K_2CO_3 (2.0 equiv)/70 °C/3 h	86	10
11	Pd@gel-Fe₃O₄	1 mol% catalyst/MeOH/Na_2CO_3 (3.0 equiv)/60 °C/5 h	89	11
12	Pd/TiO₂	0.7 mol% catalyst/NMP: H_2O (2.5: 1)/Na_2CO_3 (1.5 equiv)/120 °C/4 h	91	12
13	Pd/Fe₃O₄ NPs	0.2 mol% catalyst/MeOH/K_2PO_3 (3.0 equiv)/60 °C/18 h	91	13

Reference

1 S. Zheng, P. Y. Yang, F. M. Zhang, D. L. Chen and W. D. Zhu, *Chem. Eng. J.*, 2017, **328**, 977–987.

2 Z. J. Wang, J. J. Lv, J. J. Feng, N. B. Li, X. H. Xu, A. J. Wang and R. H. Qiu, *RSC Adv.*, 2015, **5**, 28467–28473.

3 J. C. Park, E. Heo, A. Kim, M. Kim, K. H. Park and H. Song, *J. Phys. Chem. C*, 2011, **115**, 15772–15777.

4 S. Zhang, J. Li, W. Gao and Y. Q. Qu, *Nanoscale*, 2015, **7**, 3016–3021.

5 L. Zhong, A. Chokkalingam, W. S. Cha, K. S. Lakhi, X. Y. Su, G. Lawrence and A. Vinu, *Catal. Today*, 2015, **243**, 195–198.

6 Q. Cai, G. S. Liang, Y. F. Xu, X. H. Qian and W. P Zhu, *RSC Adv.*, 2016, **6**. 60996–61000.

7 J. Wang, J. Bai, H. Liang and C. Li, *Colloids Surf. A*, 2019, **572**, 283–289.

8 N. Kim, M. S. Kwon, C. M. Park and J. Park, *Tetrahedron Lett.*, 2004, **45**, 7057–7059.

9 P. Han, X.M. Wang, X.P. Qiu, X.L. Ji and L.X. Gao, *J. Mol. Catal. A-Chem.* 2007, **272**, 136–141.

10 L. X. You, W. H. Zong, G. Xiong, F. Ding, S. J. Wang, B. Y. Ren, I. Dragutan, V. Dragutan and Y. G. Sun, *Appl. Cata. A-Gen.*, 2016, **511**, 1–10.

11 Y. T. Liao, L. S. He, J. Huang, J. Y. Zhang, L. Zhuang, H. Shen and C. Y. Su, *ACS Appl. Mater. Interfaces*, 2010, **2**, 2333–2338.

12 M. Nasrollahzadeh and S. M. Sajadi, *J. Colloid. Interf. Sci.*, 2016, **465**, 121–127.

13 M. Nasrollahzadeh, S. M. Sajadi, A. Rostami-Vartooni and M. Khalaj, *J. Mol. Catal. A-Chem.*, 2015, **396**, 31–39.

Analytical data of the products

biphenyl
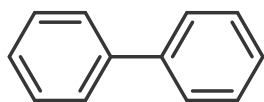
^{1}H NMR (600 MHz, CDCl$_3$) δ=7.89–7.73 (m, 1H), 7.71–7.58 (m, 1H), 7.61–7.40 (m, 1H). ^{13}C NMR (151 MHz, CDCl$_3$) δ=141.41 (s), 128.96 (s), 128.78 (s), 127.40 (d, J=14.0).

2-biphenylcarboxaldehyde
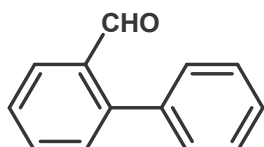
^{1}H NMR (600 MHz, CDCl$_3$) δ=10.02 (s, 1H), 8.07 (dd, J=7.8, 1.1, 1H), 7.66 (td, J=7.5, 1.3, 1H), 7.58–7.44 (m, 5H), 7.44–7.37 (m, 2H). ^{13}C NMR (151 MHz, CDCl$_3$) δ 192.44, 145.99, 137.77, 133.74, 133.60, 130.82, 130.14, 128.47, 128.16, 127.81, 127.59.

4-biphenylcarboxaldehyde
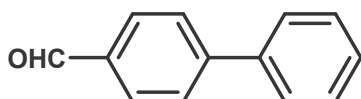
^{1}H NMR (600 MHz, CDCl$_3$) δ=10.05 (s, 1H), 7.95 (d, J=8.0, 2H), 7.74 (d, J=8.0, 2H), 7.64 (d, J=7.5, 2H), 7.47 (dt, J=33.0, 7.3, 3H). ^{13}C NMR (151 MHz, CDCl$_3$) δ=191.98 (s), 147.11 (s), 139.66 (s), 135.70 (s), 135.23 (s), 132.75 (s), 130.32 (s), 129.10 (s), 128.57 (s), 128.00 (d, J=18.7), 127.67 (s), 127.40 (s), 127.18 (s).

4-methoxybiphenyl
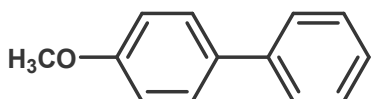
^{1}H NMR (600 MHz, CDCl$_3$) δ=7.67–7.59 (m, 1H), 7.50 (s, 1H), 7.39 (t, J=7.4, 1H), 7.06 (d, J=8.7, 1H), 3.91 (s, 1H). ^{13}C NMR (151 MHz, CDCl$_3$) δ=159.22 (s), 140.89 (s), 133.83 (s), 128.81 (s), 128.23 (s), 126.78 (d, J=9.9), 114.28 (s), 55.39 (s).

2-phenyltoluene
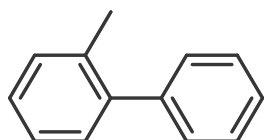
^{1}H NMR (600 MHz, CDCl$_3$) δ=7.77–7.35 (m, 1H), 2.67–2.48 (m, 1H). ^{13}C NMR (151 MHz, CDCl$_3$) δ = 142.21 (t, J=5.7), 135.53 (d, J=2.7), 130.55 (d, J=4.6), 130.05 (d, J=4.6), 129.43 (d, J=4.4), 128.98 (s), 128.31 (d, J=4.6), 127.50 (d, J=4.7), 127.00 (d, J=4.3), 126.03 (d, J=5.0), 20.73 (s).

4-phenyltoluene
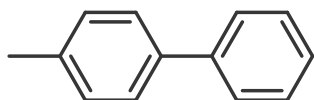
^{1}H NMR (600 MHz, CDCl$_3$) δ=7.74 (dd, J=8.3, 1.2, 1H), 7.66 (d, J=8.1, 1H), 7.58 (t, J=7.8, 1H), 7.48 (s, 1H), 7.40 (d, J=7.9, 1H), 2.55 (s, 2H). ^{13}C NMR (151 MHz, CDCl$_3$) δ=141.32 (s), 138.51 (s), 137.13 (s), 129.64 (s), 128.87 (s), 128.69 (s), 127.34–127.06 (m), 126.96 (s), 21.24 (s).

4-nitrobiphenyl
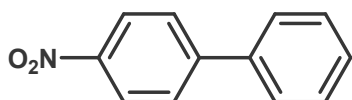
^{1}H NMR (600 MHz, CDCl$_3$) δ 8.35–8.30 (m, 1H), 7.78–7.74 (m, 1H), 7.67–7.64 (m, 1H), 7.55–7.45 (m, 2H), 7.28 (s, 1H). ^{13}C NMR (151 MHz, CDCl$_3$) δ 147.66 (s), 138.79 (s), 129.17 (s), 128.93 (s), 127.82 (s), 127.40 (s), 124.13 (s).

Figs. S14-S19 ^{1}H and ^{13}C NMR spectra of coupling products.

Fig. S14 ^{1}H and ^{13}C NMR spectra for biphenyl.
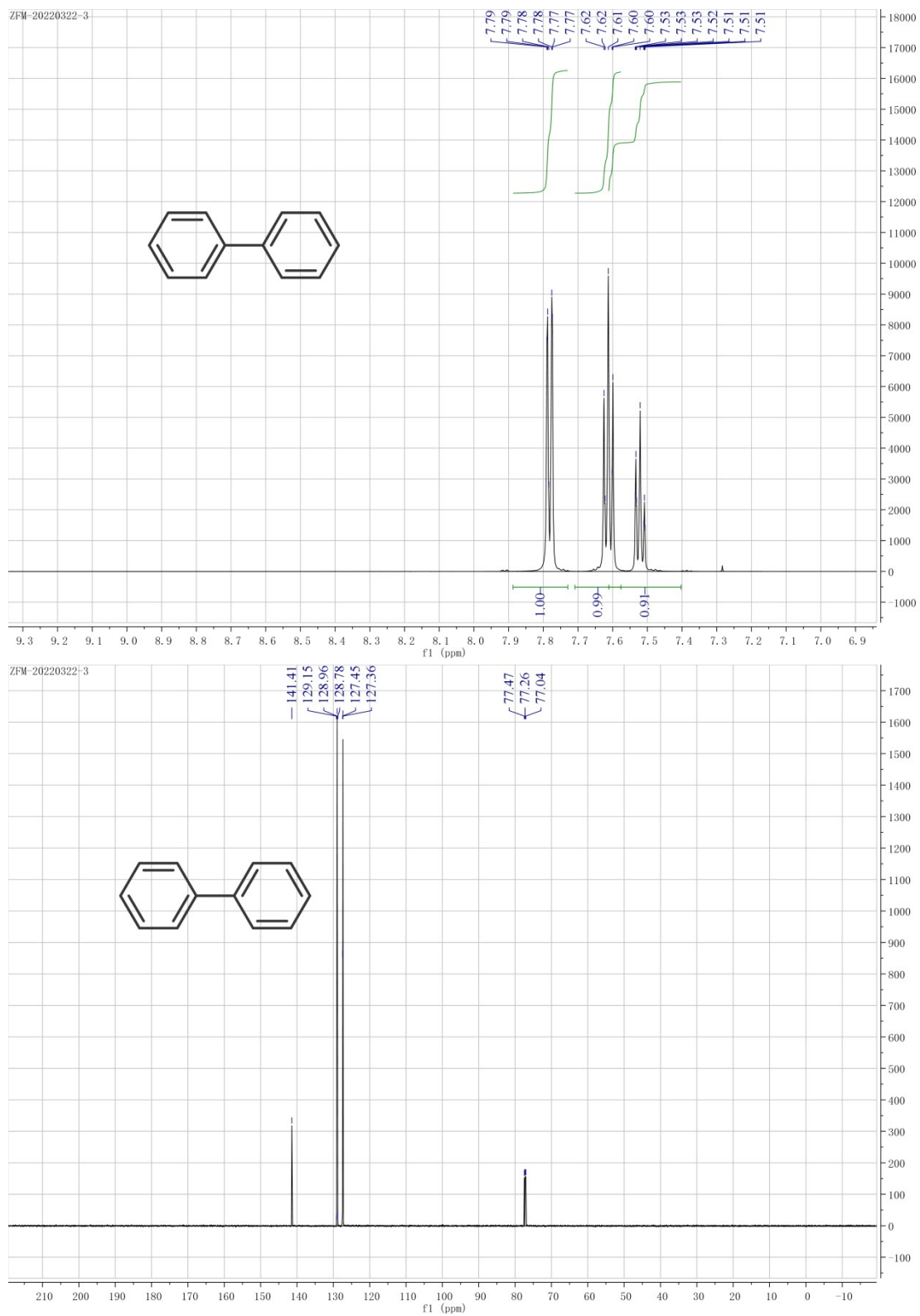
Fig. S15 ^{1}H and ^{13}C NMR spectra for 2-biphenylcarboxaldehyde.
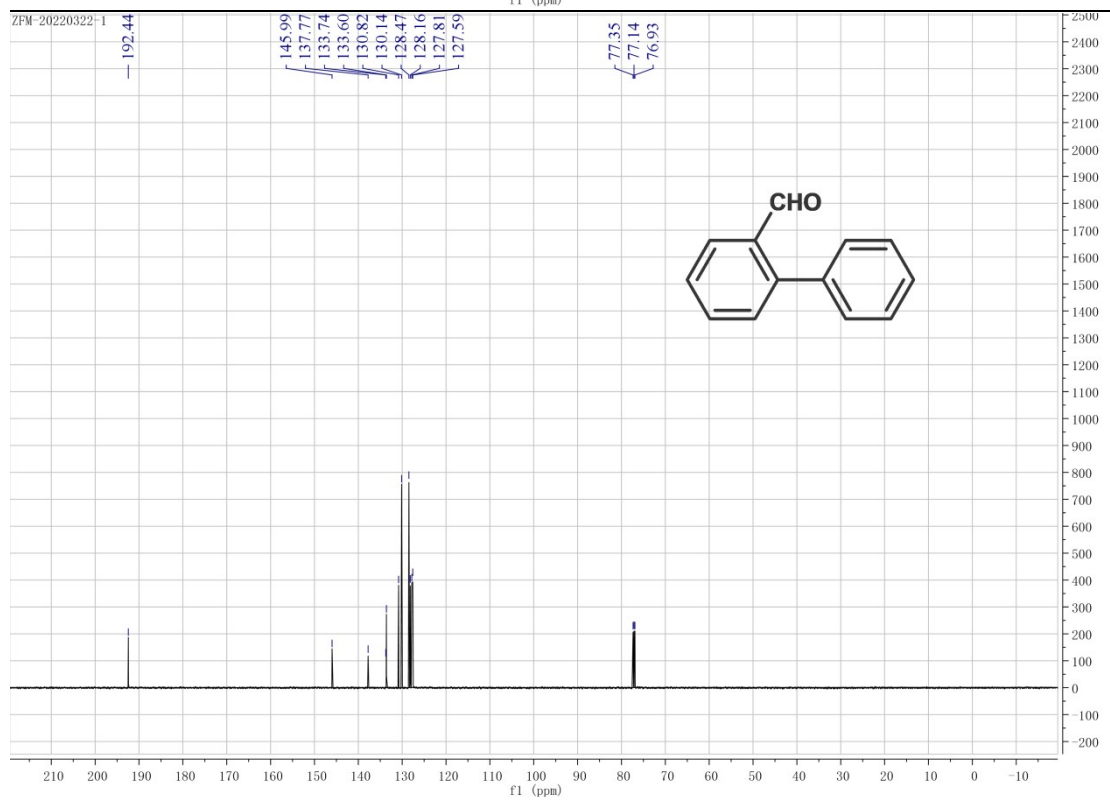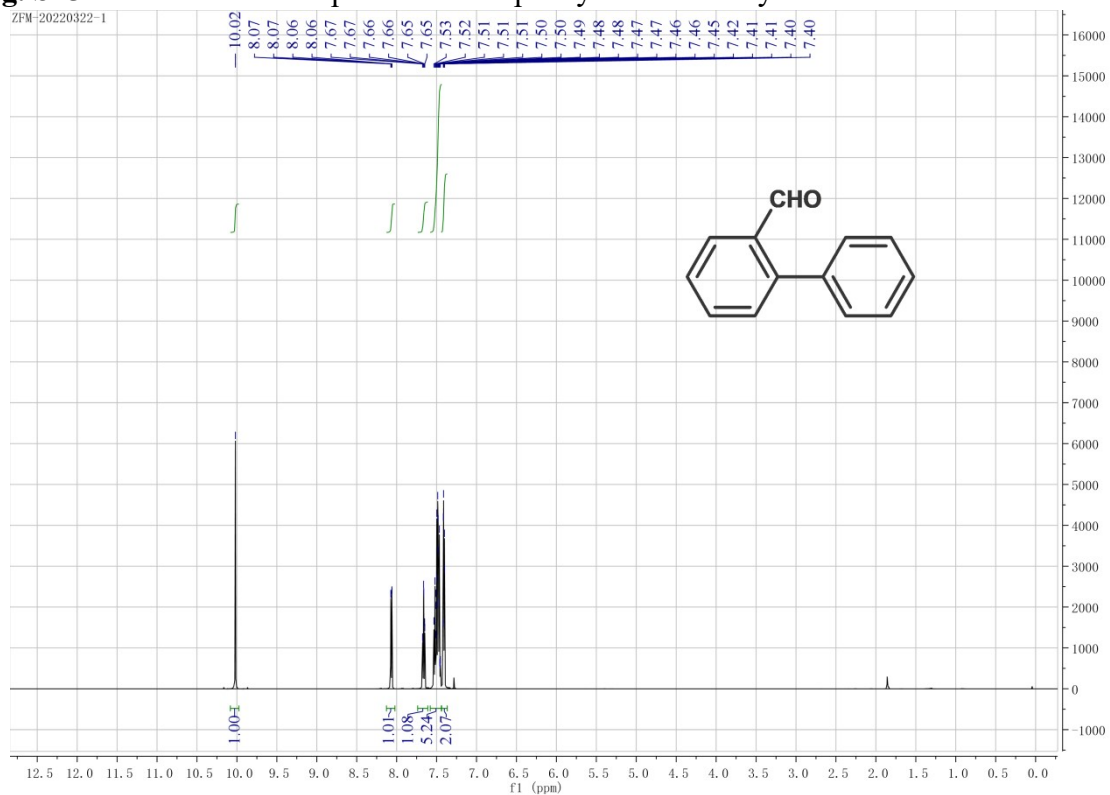
Fig. S16 ^{1}H and ^{13}C NMR spectra for 4-biphenylcarboxaldehyde.
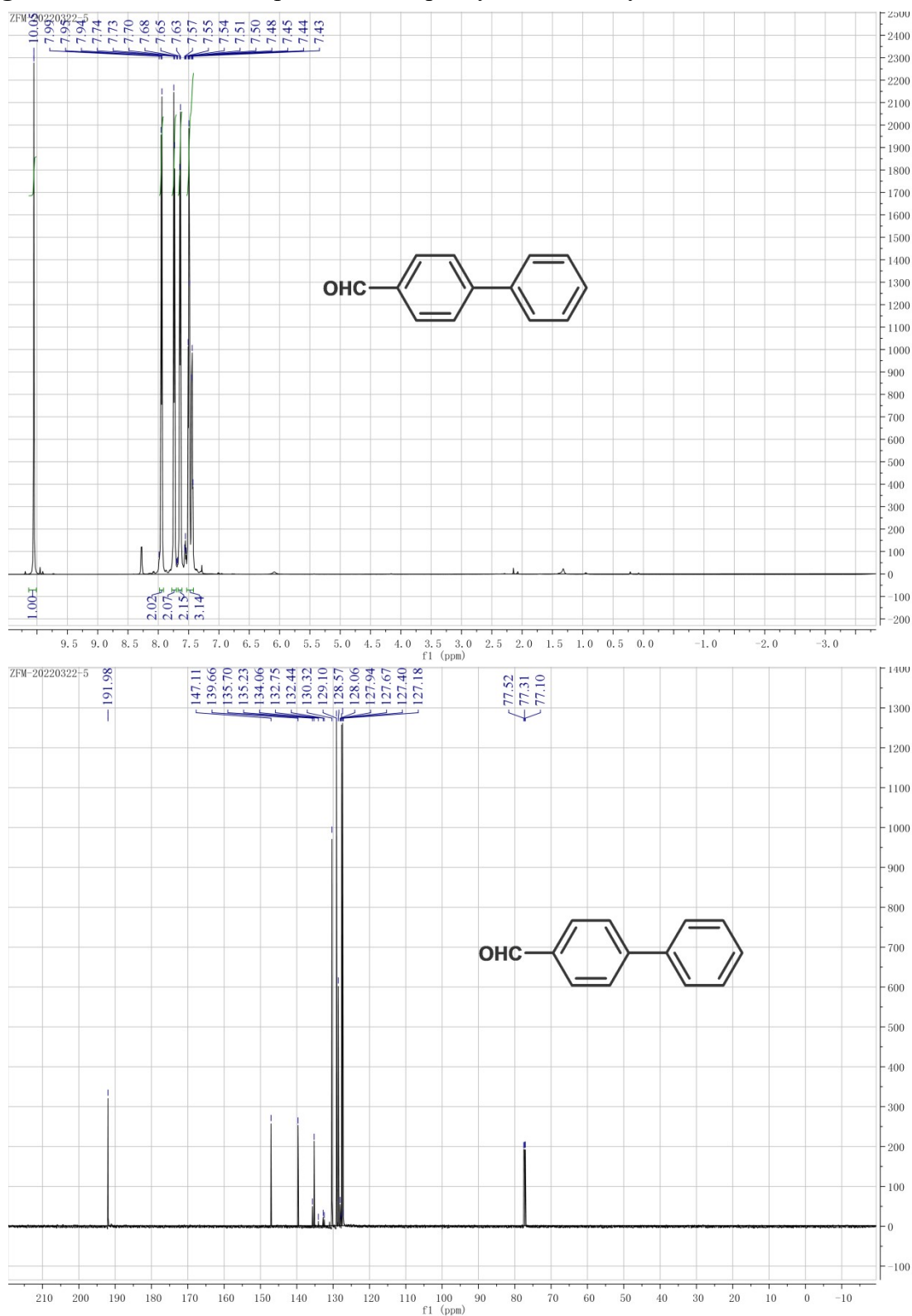
Fig. S17 ^{1}H and ^{13}C NMR spectra for 4-methoxybiphenyl.
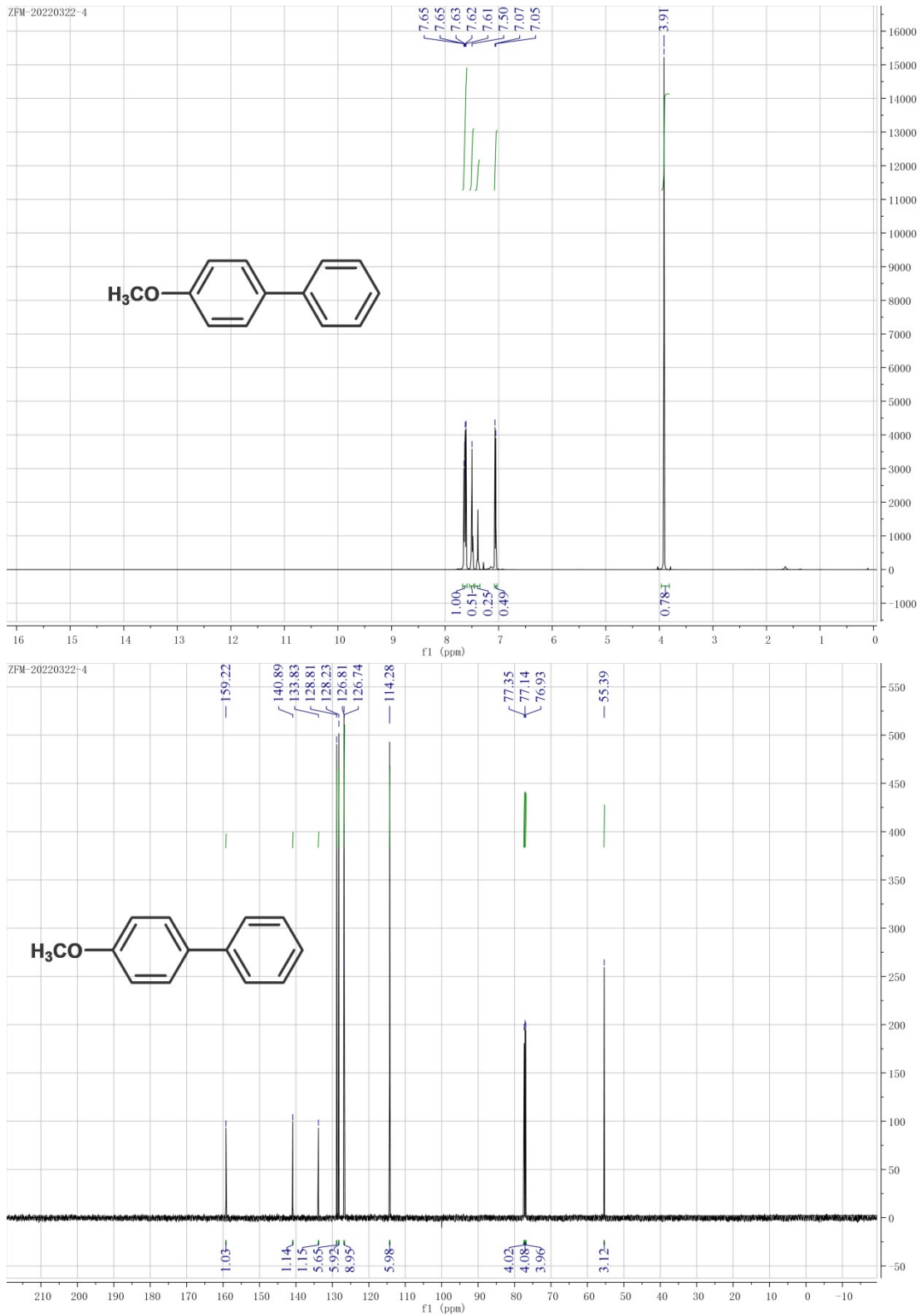
Fig. S18 ^{1}H and ^{13}C NMR spectra for 2-phenyltoluene.
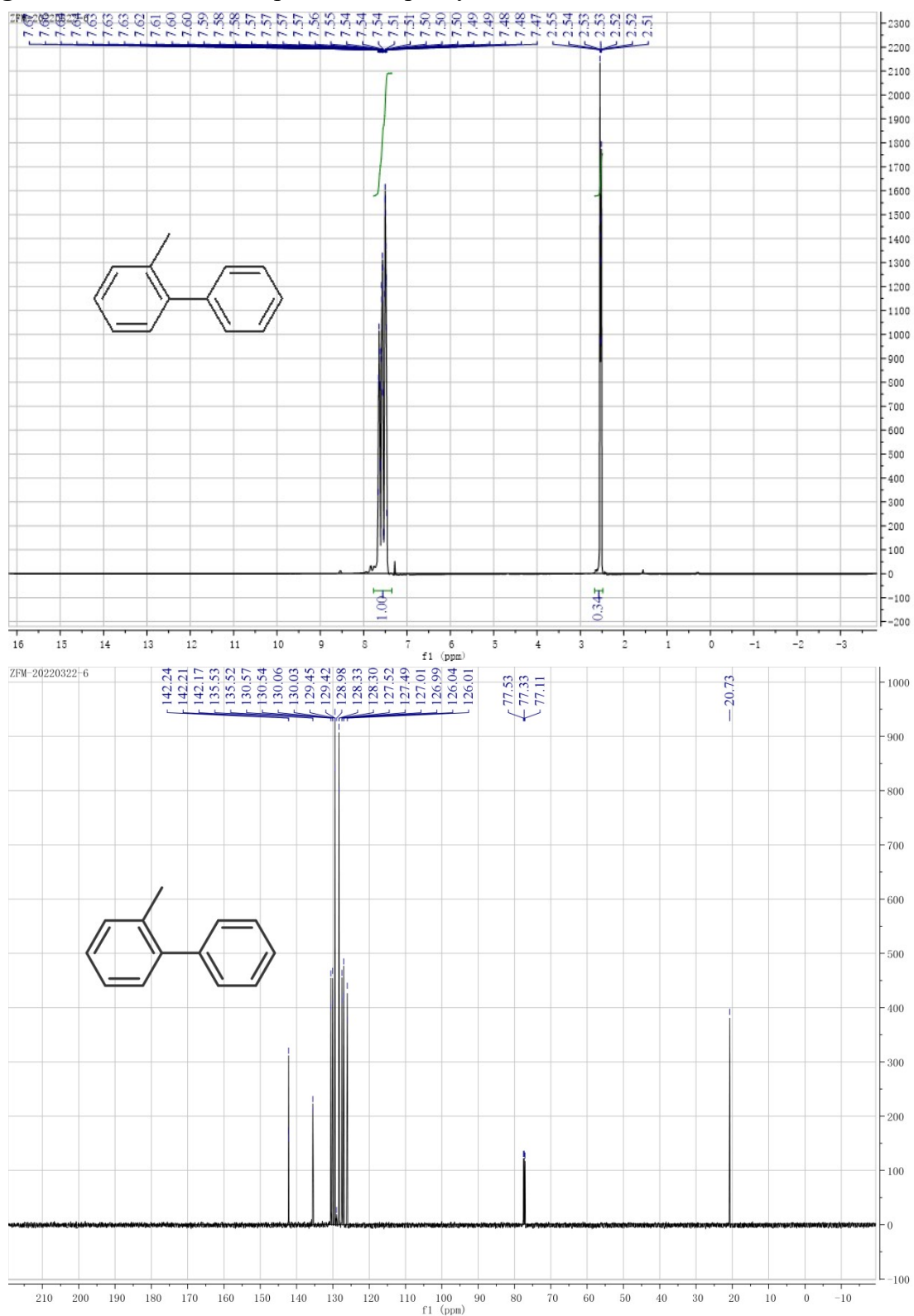
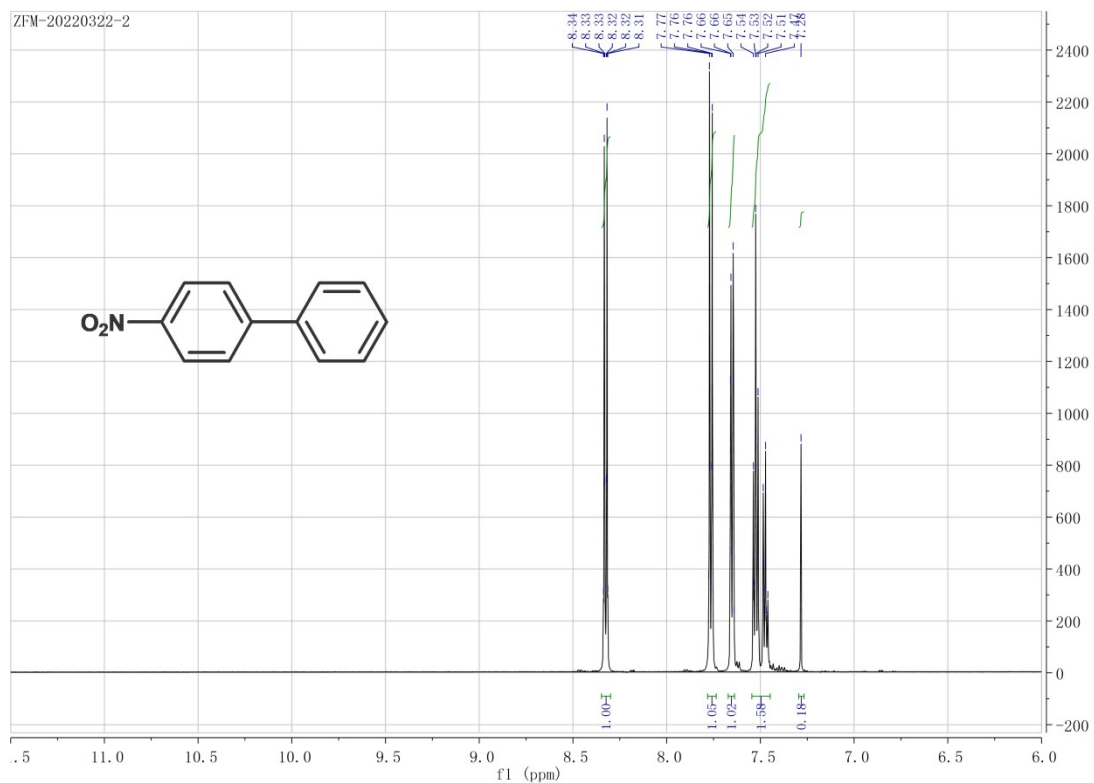**Fig. S19** ^{1}H and ^{13}C NMR spectra for 4-phenyltoluene.
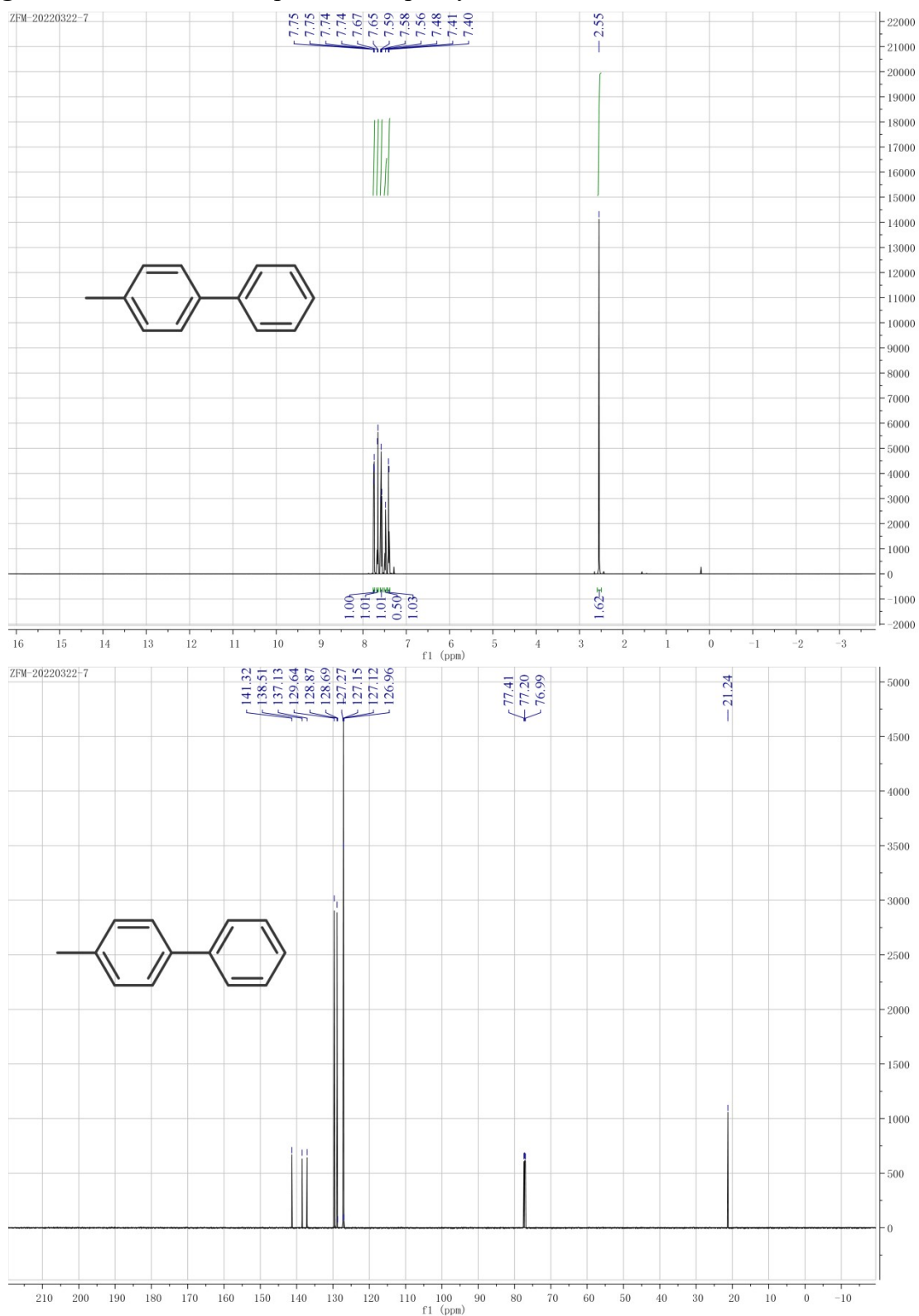
Fig. S20 ^{1}H and ^{13}C NMR spectra for 4-nitrobiphenyl.
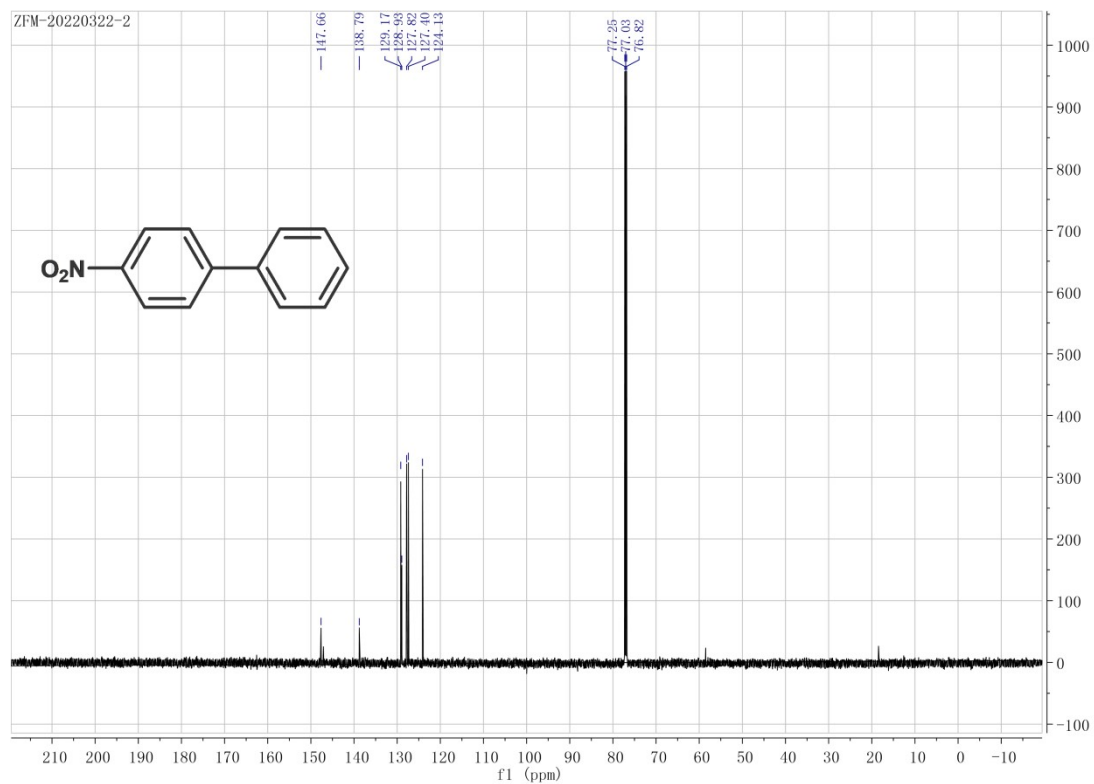
MS spectra

Fig. S21 MS spectra of the biphenyl.
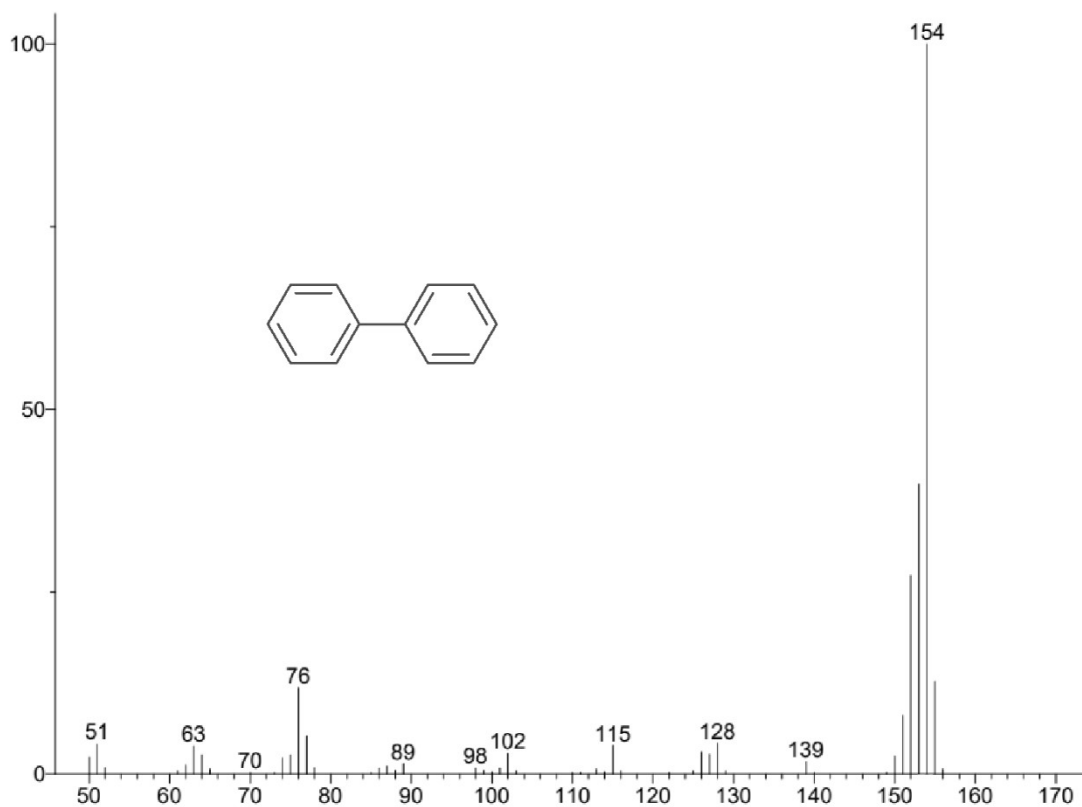
Fig. S22 MS spectra of the 2-biphenylcarboxaldehyde.
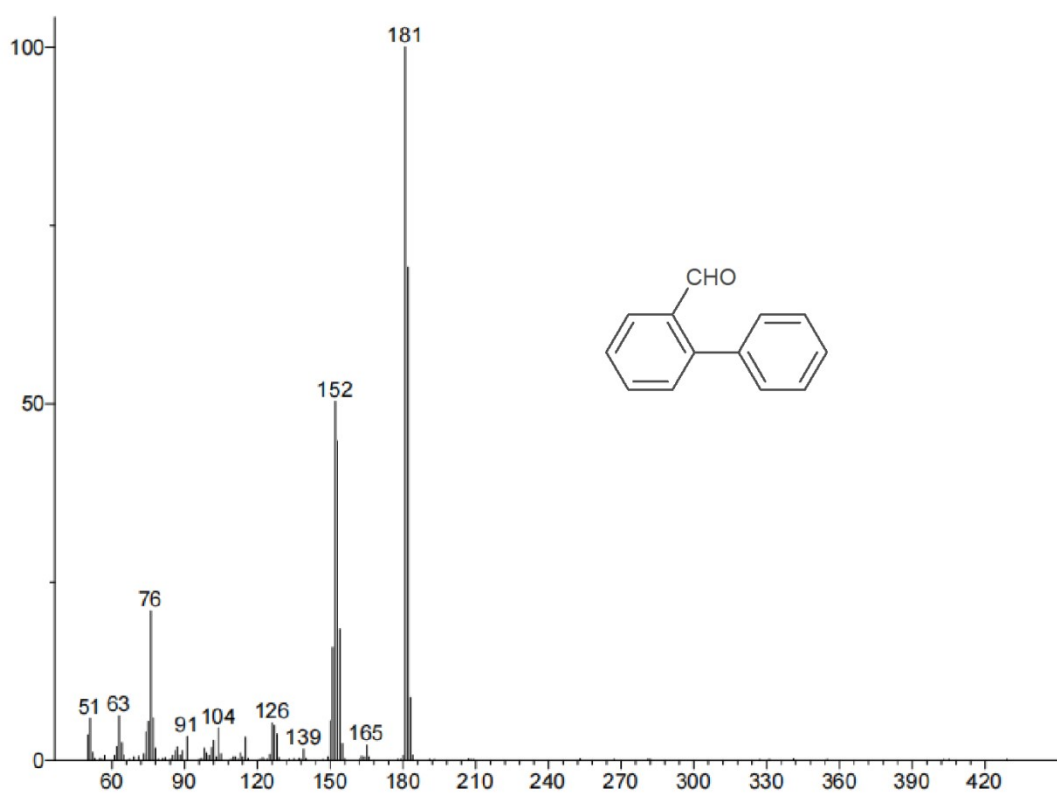
Fig. S23 MS spectra of the 3-biphenylcarboxaldehyde.
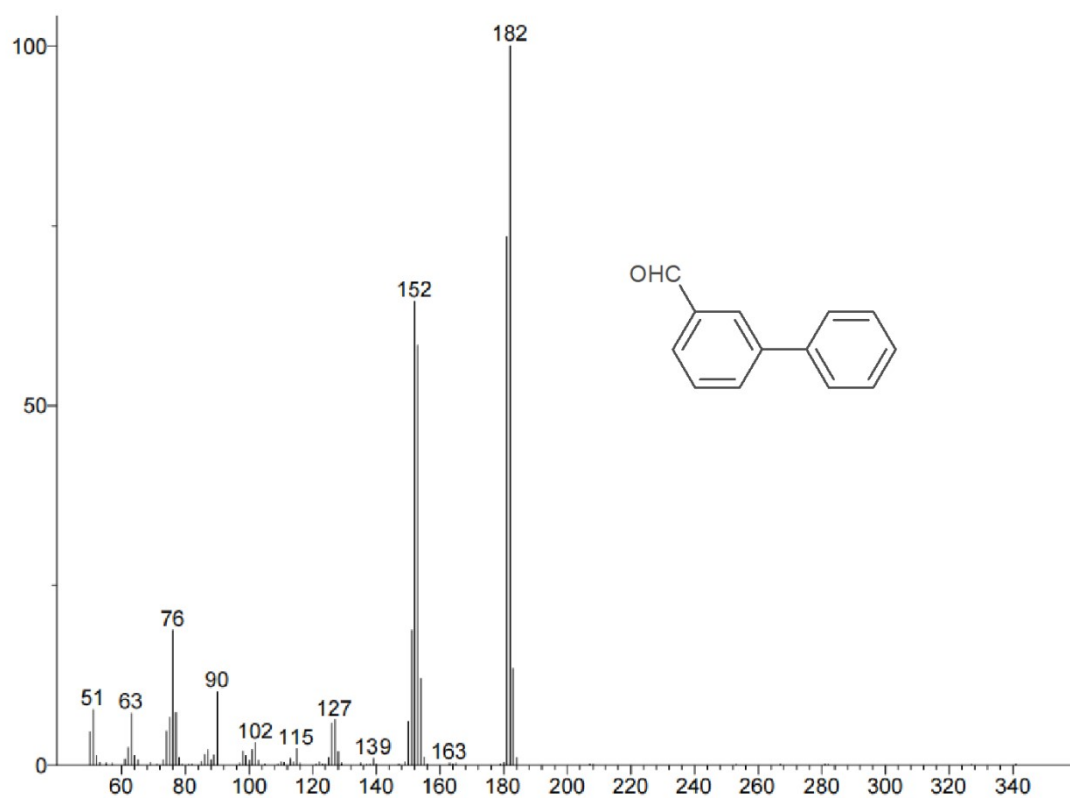
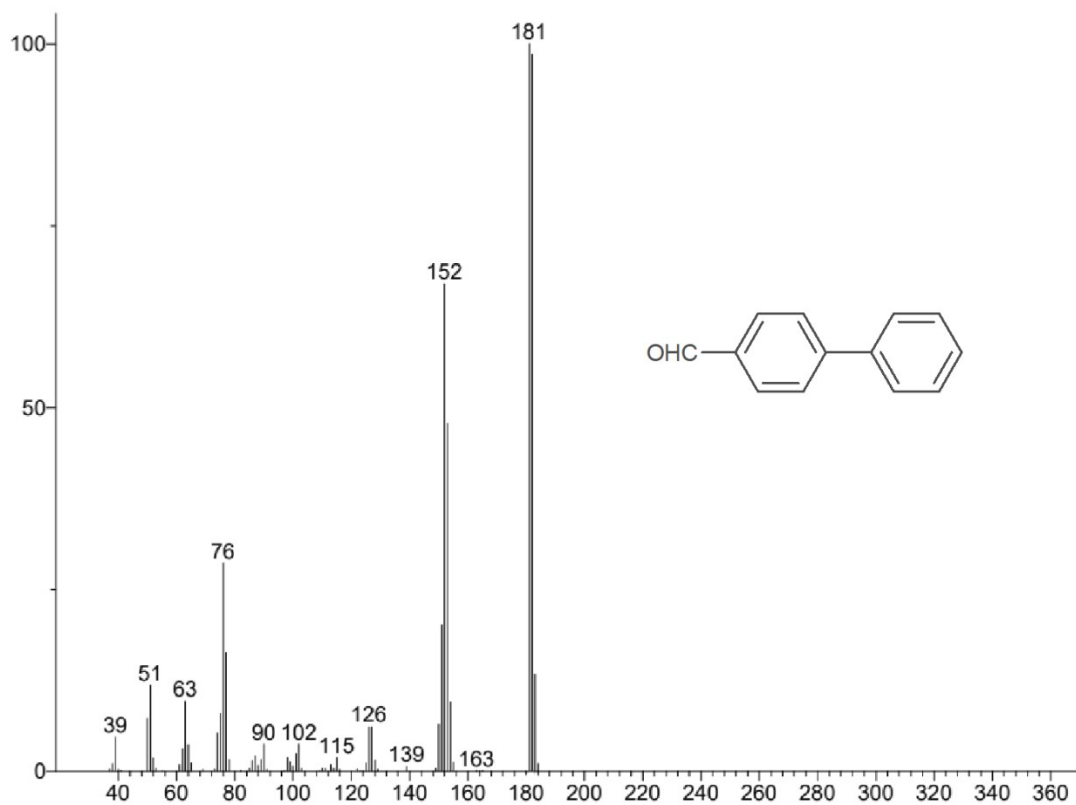**Fig. S24** MS spectra of the 4-biphenylcarboxaldehyde.
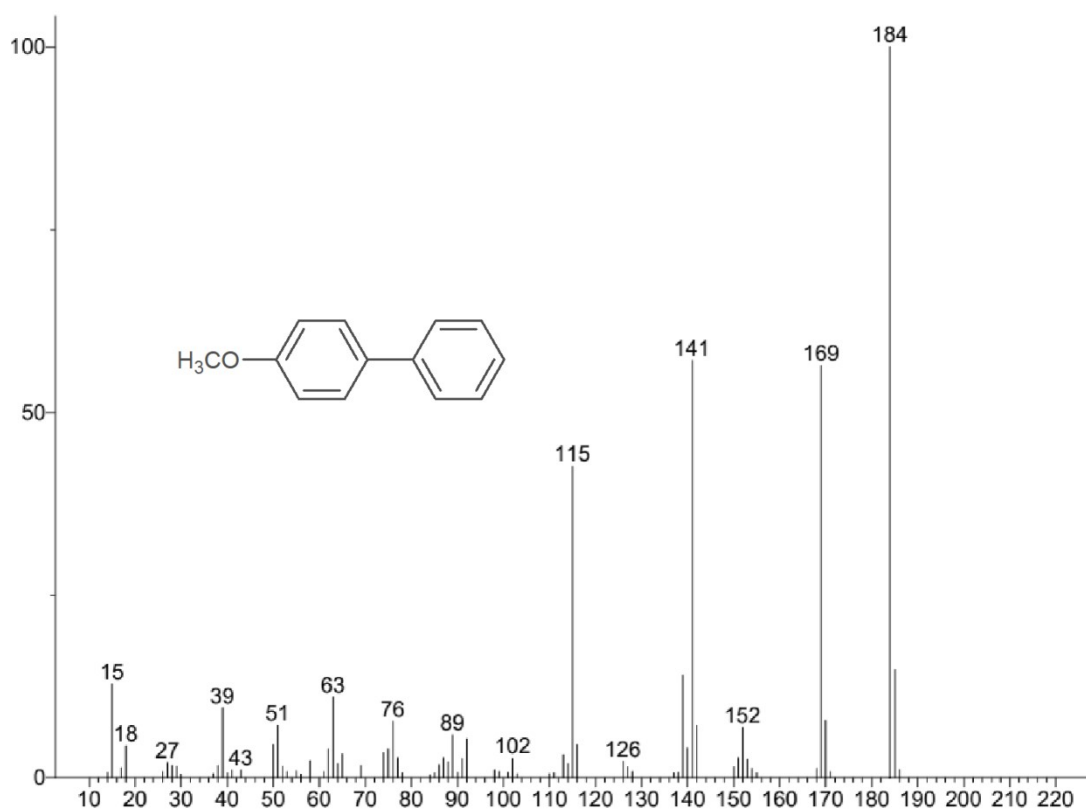
Fig. S25 MS spectra of the 4-methoxybiphenyl.

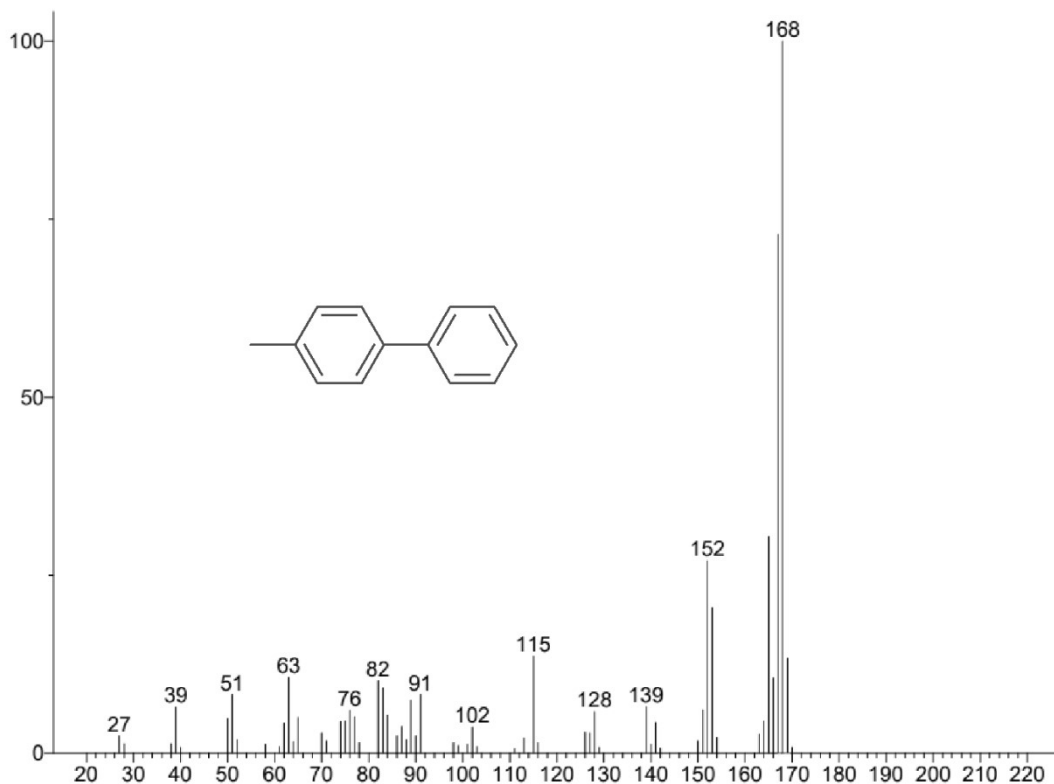**Fig. S26** MS spectra of the 4-phenyltoluene.
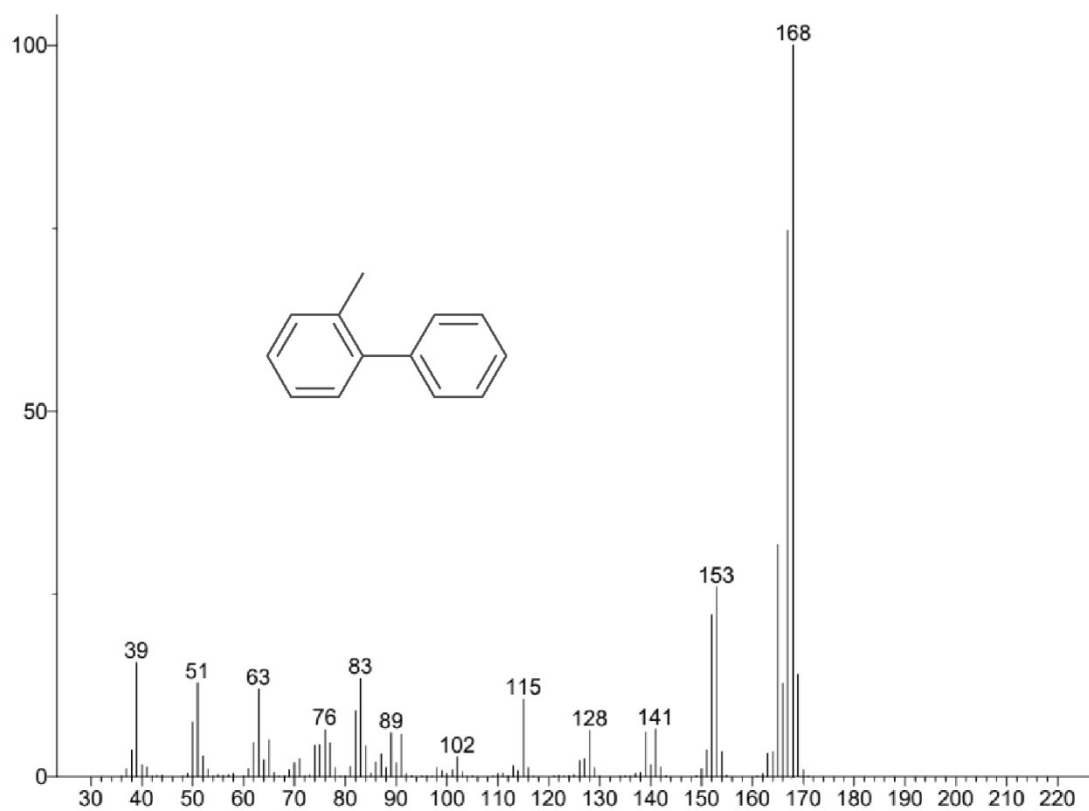
Fig. S27 MS spectra of the 2-phenyltoluene.

Fig. S28 MS spectra of the 4-nitrobiphenyl.